Energy Reports 13 (2025) 6079–6088

Contents lists available at ScienceDirect

Energy Reports

journal homepage: www.elsevier.com/locate/egyr

Research paper

Thermochemical simulations of hydrogen production from polypropylene plastic waste coupled with methanation of CO & CO_2 from steelmaking off-gases

Azita Etminan [a,*], Peter J. Holliman [a], Ian Mabbett [a], Ciaran Martin [b], Chay Davies-Smith [b]

[a] Faculty of Science and Engineering, Bay Campus, Swansea University, Swansea SA1 8EN, UK
[b] Tata Steel UK, Port Talbot, UK

ARTICLE INFO

Keywords:
Steel off-gas
Polypropylene (PP) pyrolysis
Gibbs free energy minimization
Thermodynamic optimization
Hydrogen production
Methane synthesis

ABSTRACT

Industrial decarbonization requires scalable pathways to recycle carbon-rich waste and produce low-emission fuels. Steelmaking emits substantial CO and CO_2 via off-gases, while plastic waste particularly polypropylene (PP) offers a hydrogen-rich feedstock. This work presents a thermodynamic simulation that employs Gibbs free energy minimization to optimize methane synthesis from steelmaking off-gases (CO and CO_2). The process is driven by hydrogen produced through polypropylene ($(–C_3H_6–)_n$, PP) pyrolysis, enabling the conversion of two industrial waste streams into synthetic methane (CH_4). Energy and exergy efficiencies were evaluated to assess the viability and performance of this integrated approach. PP pyrolysis at 650 °C and 1 bar was found to yield 7 mol h^{-1} of H_2, achieving energy and exergy efficiencies of 65 % and 35 %, respectively. This H_2 was directly coupled to methanation of CO and CO_2 at 250 °C and 10 atm, yielding CH_4 with an 82 % selectivity and complete (100 %) conversion of both carbon sources. The methanation step displayed peak energy and exergy efficiencies near 78 %, while coke formation remained suppressed due to effective carbon reconversion at $\leq$ 300 °C. The synergy process enables enhanced thermodynamic performance and system integration, transforming waste plastics and metallurgical off-gases into clean, usable fuels. The combined pathway offers a circular, low-carbon solution for hydrogen and methane synthesis using industrial residues, supporting both energy transition goals and waste management.

1. Introduction

The reduction of carbon dioxide (CO_2) and carbon monoxide (CO) emissions from industrial processes, particularly from steel manufacturing, remains a major challenge in the global transition toward sustainable energy systems (Bailera et al., 2021; Kim et al., 2022; Bampaou et al., 2022). Recent research has explored various advanced approaches, including electrochemical CO_2 reduction in molten salts (Al-Juboori et al., 2020), chemical looping (Najera et al., 2011), and catalytic conversion technologies (Alper and Orhan, 2017) which aim to transform these gases into value-added fuels and chemicals. Notably, electrochemical reduction in molten salts at temperatures above 700 °C offers high selectivity and efficiency for sustainable fuel production (Han et al., 2023), with the added benefit of in-situ CO_2 capture (Jia et al., 2024), However, issues such as short-circuiting due to carbon deposition remain (Zhu et al., 2023). Additionally, Chemical looping methods have also demonstrated promise for CO_2 valorization, facilitating closed-loop carbon cycles in fuels and materials (Zhou et al., 2023; Jin et al., 2023). Recent advances in heterogeneous catalysis have further improved CO_2 and CO conversion to methane, methanol, and syngas (Usman et al., 2023). Metal-organic frameworks (MOFs) and perovskite oxides, in particular, exhibit high activity and selectivity under mild conditions (Jiang et al., 2024; Sani et al., 2023; Zhao et al., 2023). Despite these improvements, catalytic CO_2 hydrogenation systems continue to face challenges regarding catalyst efficiency, stability, and cost.

A critical limiting factor in these systems is the availability of sustainable hydrogen (H_2), which acts as a key reductant in CO_2 and CO methanation reactions (Saeidi et al., 2021; Hussain et al., 2021). While several low-carbon H_2 production technologies are under development including alkaline electrolysis (AEL), polymer electrolyte membrane electrolysis (PEMEL), high-temperature electrolysis (HTEL), steam

* Corresponding author.
E-mail address: 2157090@swansea.ac.uk (A. Etminan).

https://doi.org/10.1016/j.egyr.2025.05.043
Received 19 December 2024; Received in revised form 14 May 2025; Accepted 15 May 2025
Available online 24 May 2025

methane reforming with carbon capture (SMR-CCUS), and methane pyrolysis each presents economic or operational trade-offs (Younas et al., 2022; Zhang et al., 2024). For instance, AEL is cost-effective, PEMEL is highly adaptable to renewable inputs, and HTEL offers high efficiency but relies on expensive materials. SMR-CCUS remains the most established option at scale but continues to emit CO_2 even with carbon capture (Dermühl and Riedel, 2023). Methane pyrolysis, powered by renewable energy, shows considerable promise as a low-emission alternative but faces challenges such as catalyst deactivation and high energy demands (Patlolla et al., 2023). Biomass gasification is also being investigated as a feedstock-flexible route for H_2 generation, though it can be energy-intensive and produce CO_2 emissions (Chen et al., 2024; Rubinsin et al., 2024).

Polypropylene (PP), a major component of plastic waste, presents a hydrogen-rich feedstock for thermochemical conversion via pyrolysis. This dry process generates H_2 and carbonaceous gases without the need for water or oxygen, offering a potentially sustainable pathway for decentralized H_2 production, especially when powered by renewable energy (Wu and Williams, 2009; Liu et al., 2011). However, most studies to date have treated H_2 production from plastic pyrolysis and CO_2/CO conversion via methanation as separate processes, overlooking potential synergies between the two. By comparison, integrating H_2 production with carbon utilization offers a strategic path toward a sustainable, low-carbon economy (Varvoutis et al., 2022; Aresta and Dibenedetto, 2024). By combining CO_2 with renewable H_2 (Green-H_2 or Blue-H_2), fuels like methane and methanol can be synthesized, which are easier to store and transport than H_2 (Aresta and Dibenedetto, 2024). Methane and methanol, synthesized by combining CO_2 with renewable H_2, are easier to store and transport than H_2 itself, making such integration attractive for near-term industrial decarbonization. This approach aligns with circular economy principles and supports global efforts toward net-zero carbon emissions (Aresta and Dibenedetto, 2024).

In this study, we develop a thermodynamically integrated pathway that couples' hydrogen production from polypropylene pyrolysis with the methanation of CO and CO_2 present in steelmaking off-gases. While previous research has examined these processes separately, their combined application within a unified system has not been systematically addressed. Using Gibbs free energy minimization, we determine optimal operating conditions that enable complete carbon conversion and efficient hydrogen utilization under catalyst-free conditions. This integrated approach establishes a closed-loop valorization route for plastic waste and metallurgical emissions, offering a scalable strategy for low-carbon synthetic methane production in energy-intensive industries.

2. Methodology

Blast Furnace Gas (BFG) and Basic Oxygen Furnace Gas (BOFG) were selected as primary sources of CO and CO_2 feedstock for methanation, with their compositions listed in Table 1. Clean gas conditions were assumed, and simulations were conducted in the absence of catalysts to isolate and evaluate the thermodynamic potential and process efficiencies under idealized conditions. Polypropylene (PP) was employed as the plastic waste feedstock for hydrogen production via pyrolysis. The pyrolysis product composition values for polypropylene (PP) listed in Table 1 were derived from Gibbs free energy minimization at T = 650 °C and P = 1 bar. The gas-phase concentrations reflect thermodynamic equilibrium outcomes under ideal conditions, and do not include kinetic or catalytic effects. Therefore, some uncertainty in the product distribution may be expected, particularly for minor hydrocarbon species. Thermodynamic modelling was carried out using licensed HSC Chemistry (v10, Outotec), enabling Gibbs free energy minimization to optimize H_2 production from PP pyrolysis and CO/CO_2 methanation from steelmaking off-gases, while minimizing carbon formation. The basic chemical properties and thermodynamic behaviour of polypropylene including enthalpy, entropy, heat capacity, and Gibbs free energy are summarized in the Supporting Information (Fig. S1 and Table S1), providing the foundational data for the pyrolysis modelling.

2.1. Gibbs free energy minimization

The reaction equation and equilibrium composition modules within HSC Chemistry software were used to determine the equilibrium constants and compositions for selected reactions versus temperature. The computation of the Gibbs free energy $\Delta_r G^\circ$ (T) and equilibrium constants K_p (T) are represented by the following equations (Khor et al., 2022; Kakoee and Gharehghani, 2020):

$$Kp = \exp\left(\frac{-\Delta rG(T)}{RT}\right) \tag{1}$$

$$\Delta rG^\circ(T) = \Delta rH^\circ(T) - T\Delta rS^\circ(T) \tag{2}$$

$$\Delta rH^\circ(T) = \Delta rHm(T) + \int_{298}^{T} \Delta rCp, mdT \tag{3}$$

$$\Delta rS^\circ(T) = \Delta rSm(T) + \int_{298}^{T} \Delta rCp, m\frac{dT}{T} \tag{4}$$

3. Energy and exergy balance

Energy, exergy and system heat loss calculations, for both pyrolysis and methanation processes, were extracted from the HSC software. This study focuses exclusively on the exergy efficiency of gas products relative to the reactant exergy, temporarily excluding the exergy of carbon products and exergy losses from the analysis. This simplification was applied to isolate the thermodynamic behavior of gas-phase components directly involved in hydrogen production and methanation processes. Similarly, exergy losses were excluded to preserve a theoretical performance benchmark under idealized conditions. Future system-scale studies may incorporate these effects to provide a more

Table 1
Composition (%vol) of main components of dry steel making and pyrolysis gases.

Blast Furnace Gas (BFG)							
CO	CO_2	H_2	N_2		H_2S + COS (ppm)	Lower Heating Value (LHV) ($MJ.m^3$)	Ref
23.50	21.60	3.70	46.60		0.4	4.20	(Angeli et al., 2021)
23.80	22.60	3.70	49.90		-	4.50	(Hos and Herskowitz, 2021)
25.00	23.00	4.00	48.00		0.00	3.40	(Büker et al., 2022)
Basic Oxygen Furnace Gas (BOFG)							
CO	CO_2	H_2	N_2		H_2S + COS (ppm)	Calorific Value ($MJ.m^3$)	Ref
75.00	19.00	2.00	5.00		-	9.50	(Wolf-Zoellner et al., 2021)
60.9	17.20	-	15.50		4.30	8.20	(Wolf-Zoellner et al., 2021)
54.00	20.00	4.00	18.10		3.20	7.20	(Melo Bravo et al., 2020)
Pyrolysis Products Gas							
H_2	CH_4	C_2H_6	C_3H_8	C_2H_4	Calorific Value ($MJ.m^3$)		Ref
48.48	1.52	$6.72 * 10^{-6}$	$1.7 * 10^{-10}$	$3.12 * 10^{-6}$	1.41		Table S2

comprehensive exergy accounting. Exergy efficiency provides a comprehensive measure of how effectively the system converts available energy into useful work, which makes it a valuable metric for evaluating different processes across various scenarios (García-Nieto et al., 2023; Su and Chen, 2006; Ahmadian and Schmidt, 2020). In contrast, energy efficiency is particularly relevant in situations where the energy input is predominantly thermal (Zhang et al., 2020; Martínez-Rodríguez and Abánades, 2020).

Energy efficiency (η_{En}^{Total}) for an endothermic reaction is calculated using the following equations (Mendoza-Hernandez et al., 2019; Zhang et al., 2020):

$$Total\ Energy\ Input = \sum n_{reactants} \times H_{reactant} + Q_{heat} \tag{5}$$

$$Total\ Energy\ Output = \sum n_{products} \times H_{products} \tag{6}$$

$$\eta_{En}^{Total} = \frac{Total\ Energy\ output}{Total\ Energy\ input} \times 100 \tag{7}$$

$$\eta_{En}^{CH4} = \frac{\sum n_{CH4} \times H_{CH4}}{\sum n_{H2} \times H_{H2}} \times 100 \tag{8}$$

$$\eta_{En}^{H2} = \frac{\sum n_{H2} \times H_{H2}}{\sum n_{C3H6(PP)} \times H_{C3H6(PP)}} \times 100 \tag{9}$$

where the H is the total enthalpy of the reactant and product, Q heat is the heat supplied, and n is the molar flow.

Exergy efficiency (η_{Ex}^{Total}) is defined as the ratio of exergy recovered (Ex_{out}) to exergy supplied (Ex_{in}) as follow equations:

$$\eta_{Ex}^{Total} = \frac{Ex_{,out}}{Ex_{,in}} * 100 \tag{10}$$

Where, $Ex_{,out}$ and $Ex_{,in}$ are determined from Eq. 11-14:

$$Ex_{,in} = Ex_{,reactant} + Ex_{,Q} \tag{11}$$

$$Ex_{,reactant} = \sum n_{,reactant} \times Ex,Ch_{reactant} + \sum n_{,reactant} \times Ex,Ph_{reactant} \tag{12}$$

$$Ex,Q = Q_{heat}\left(1 - \frac{T^0}{T}\right) \tag{13}$$

$$Ex_{,out} = \sum Ex_{,Product} = \sum n_{,product} \times Ex,Ch_{Product} + n_{,product} \times Ex,Ph_{Product} \tag{14}$$

$$\eta_{Ex}^{CH4} = \frac{\sum n_{CH4} \times Ex_{CH4}}{\sum n_{H2} \times Ex_{H2}} \times 100 \tag{15}$$

$$\eta_{Ex}^{H2} = \frac{\sum n_{H2} \times Ex_{H2}}{\sum n_{C3H6(PP)} \times Ex_{C3H6(PP)}} \times 100 \tag{16}$$

Here, Ex,ch and Ex,ph are standard mole chemical exergy and physical exergy of pure substances, and Ex, Q is exergy due to heat transfer, T^0 is the reference temperature and n is the molar flow.

4. Results and discussion

4.1. Thermodynamic analysis of (-C3H6-)n pyrolysis: ΔG-Log K trends and product distribution

The pyrolysis of polypropylene $(\text{-}C_3H_6\text{-})_n$ involves several possible reactions, each producing different by-products. The primary reaction under consideration is the decomposition of $(\text{-}C_3H_6\text{-})_n$ into carbon and H_2 gas (R_1). This main reaction is endothermic, with an enthalpy change (ΔH°_{298}) of 84.471 kJmol^{-1} and a Gibbs free energy change ($\Delta G^{\circ}{}_{298}$) of −16.916 kJmol^{-1}, indicating that it is thermodynamically favorable under standard conditions. The side reactions that can occur during the pyrolysis of $(\text{-}C_3H_6\text{-})_n$ lead to the formation of various by-products as shown in Table 2, which have been reported in previous studies (Weiland et al., 2021; Mensah et al., 2022; Al-Asadi et al., 2020; Liu et al., 2020b). Table 2 shows that all reactions are endothermic. Although propylene (C_3H_6) is commonly observed as a volatile product in polypropylene pyrolysis under kinetic control, it was not present in the equilibrium compositions obtained in this study. As demonstrated by thermodynamic analysis (Fig. S2), C_3H_6 becomes unstable above ~600 °C and is predicted to decompose into smaller products such as CH_4, H_2, and C(s) under equilibrium conditions. This behavior is consistent with the Gibbs free energy minimization results produced by HSC Chemistry v10.

Fig. 1. presents the ΔG-Log K graph for the main and side reactions, illustrating the relationship between Gibbs free energy and the equilibrium constant. R_3 and R_4 are particularly notable for their significantly negative Gibbs free energy changes, indicating these reactions are also thermodynamically favorable under standard conditions. R_3 becomes more favorable at higher temperatures but is less favorable compared to the direct decomposition to carbon and H_2. R_5 remains constant in ΔG and long K across the temperature range, suggesting that it is less temperature-sensitive but generally unfavorable compared to R_4. Based on ΔG and log K provided for possible reactions in $(\text{-}C_3H_6\text{-})_n$ pyrolysis in Fig. 1, the most efficient pathway for H_2 production via pyrolysis of polypropylene appears to be the direct decomposition into carbon and hydrogen, particularly at temperatures above 650℃.

Fig. 2a. demonstrates the effect of temperature on the flow rate of products during the pyrolysis of polypropylene. The volume percentage of H_2 increases significantly with temperature, peaking around 650°C, aligning with the endothermic nature of the primary reaction. Carbon formation remains stable across the temperature range, indicating consistent production. Methane (CH_4) production increases with temperature, peaking around 500°C, suggesting favourable conditions for its formation via side reactions. Ethane (C_2H_6) and ethylene (C_2H_4) also increase with temperature, with ethylene peaking around 500°C, indicating higher temperatures facilitate these hydrocarbon formations. Propane (C_3H_8) production remains low and relatively unaffected by temperature variations, suggesting less favourable conditions for its formation. The thermodynamic analysis suggests careful temperature control can help in maximizing the production of desired H_2 product while minimizing by-product gases such as ethane, ethylene, propane or methane. The importance of temperature is supported by recent reports in catalytic technologies that enhance the efficiency and selectivity of such pyrolysis conversions (Liu et al., 2020a).

This interpretation is further supported by Liu et al. (2011), who reported that during the catalytic pyrolysis of polypropylene, hydrogen concentration in the product gas increased markedly with decomposition temperature, reaching a maximum of 72.21 vol% at 700 °C, confirming the endothermic nature of the primary decomposition reaction. In contrast, the volume percentage of propane (C_3H_8) remained consistently low across the temperature range (1.10–0.07 vol%), indicating unfavorable kinetic conditions for its formation despite possible

Table 2
Specific enthalpy, entropy and standard Gibbs free energy for polypropylene $(\text{-}C_3H_6\text{-})_n$ pyrolysis chemical reactions.

Reaction	Equation	ΔH°_{298} (kJmol^{-1})	ΔG°_{298} (kJ)	ΔS°_{298} (JK^{-1})
R_1	$(\text{-}C_3H_6\text{-})_n \rightarrow 3\ C_{(s)} + 3\ H_{2(g)}$	84.47	−16.92	340.05
R_2	$(\text{-}C_3H_6\text{-})_n \rightarrow C_{(s)} + H_{2(g)} + C_2H_{4(g)}$	136.87	51.44	286.53
R_3	$(\text{-}C_3H_6\text{-})_n \rightarrow 2\ C_{(s)} + H_{2(g)} + CH_{4(g)}$	9.87	−67.45	259.32
R_4	$(\text{-}C_3H_6\text{-})_n \rightarrow C_{(s)} + C_2H_{6(g)}$	0.79	−48.74	166.14
R_5	$2(\text{-}C_3H_6\text{-})_n \rightarrow 3\ C_{(s)} + 2\ H_{2(g)} + C_3H_{8(g)}$	64.24	−58.14	410.45

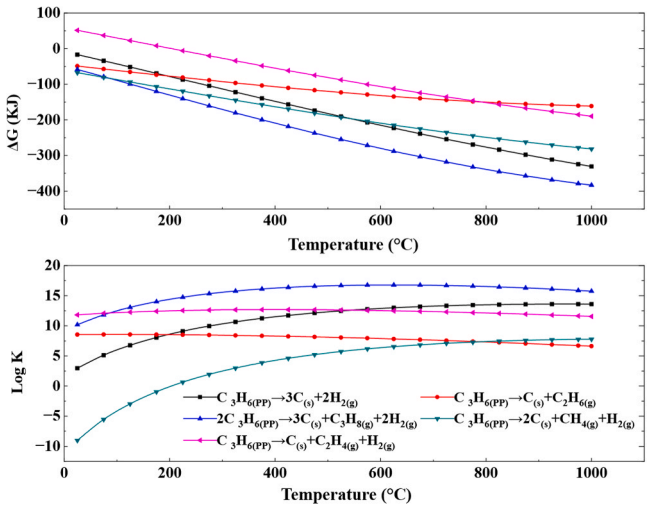

Fig. 1. ΔG-Log K versus temperature for polypropylene $(\text{-}C_3H_6\text{-})_n$ pyrolysis.

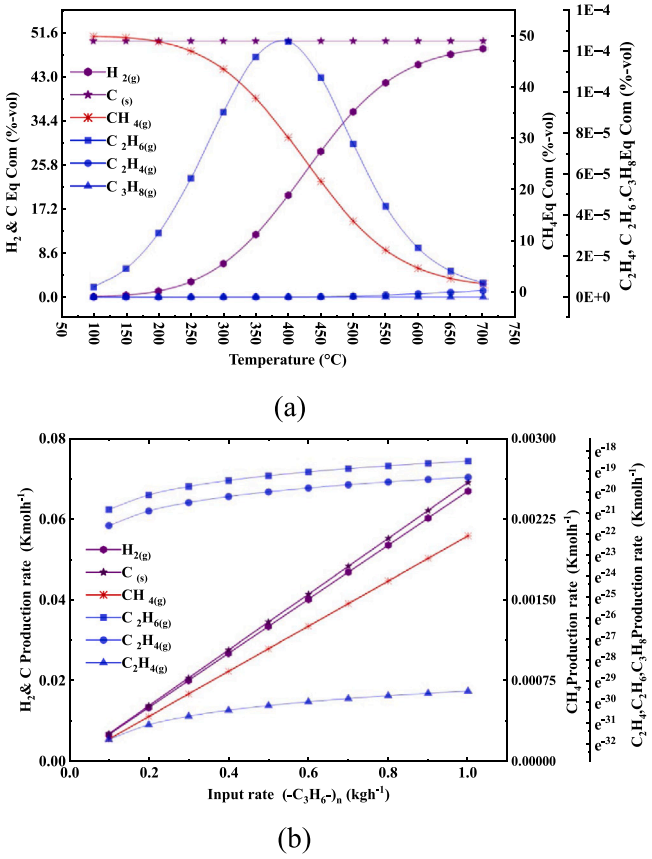

Fig. 2. The equilibrium composition of the pyrolysis reaction as influenced by (a) temperature (°C), or (b) $(\text{-}C_3H_6\text{-})_n$ flow rate(kg.h^{-1}) at P = 1 bar and T = 650°C.

thermodynamic feasibility. Methane (CH_4) and ethylene (C_2H_4) production peaked at intermediate temperatures (500–600 °C), consistent with their origin in secondary decomposition pathways that are selectively enhanced under specific thermal regimes.

Fig. 2b. illustrates that as the flow rate of $(\text{-}C_3H_6\text{-})_n$ increases, the production rates of H_2 and carbon show a linear increase, reflecting the direct stoichiometric relationship in the primary pyrolysis reaction $(\text{-}C_3H_6\text{-})_{n(s)} \rightarrow 3\ C_{(s)} + 3\ H_{2(g)}$. The production rate of methane also increases with the $(\text{-}C_3H_6\text{-})_n$ flow rate, indicating that side reactions such as $(\text{-}C_3H_6\text{-})_{n\ (s)} \rightarrow 2\ C_{(s)} + 2\ H_{2(g)} + CH_{4(g)}$ become more significant with more available propylene. Ethylene (C_2H_4) and ethane (C_2H_6) production rates similarly rise, suggesting the occurrence of reactions; $(\text{-}C_3H_6\text{-})_{n\ (s)} \rightarrow 2\ C_{(s)} + H_{2(g)} + C_2H_{4\ (g)}$ and $(\text{-}C_3H_6\text{-})_{n\ (s)} \rightarrow C_{(s)} + C_2H_{6(g)}$. However, the production of propane (C_3H_8) remains minimal across the range of C_3H_6 flow rates, indicating that the conditions at 650°C and 1 bar are not highly favorable for its formation. From a thermodynamic perspective, the primary pyrolysis reaction is the most favorable, while side reactions contribute to the formation of CH_4, C_2H_4, and C_2H_6 to a smaller amount. The consistent low production of C_3H_8 suggests kinetic limitations rather than thermodynamic constraints, as the reaction may be thermodynamically feasible but occurs at a slower rate due to less-than-ideal conditions. Studies show the decomposition of polypropylene can be significantly influenced by the reaction conditions, particularly temperature and catalyst presence, which can slow down the reaction rate even when the process is thermodynamically feasible (Kim et al., 2021).

Fig. 3. depicts the equilibrium composition of the pyrolysis reaction as a function of pressure at varying temperatures (300°C, 400°C, 500°C, and 650°C). The data reveal that hydrogen (H_2) concentration increases with temperature but consistently decreases with rising pressure at all temperatures. At 300°C, hydrogen yield is relatively low, and it declines steadily as pressure increases. This pattern continues across all temperatures, though higher temperatures (400°C to 650°C) significantly elevate overall hydrogen yield, indicating enhanced thermal cracking, but the downward trend with pressure remains evident.

In contrast, methane (CH_4) shows an inverse relationship with temperature: its concentration is highest at lower temperatures (especially 300°C and 400°C) and declines as temperature increases. However, methane content rises with pressure at every temperature. Additionally, heavier hydrocarbons such as ethane (C_2H_6), ethylene (C_2H_4), and propane (C_3H_8) begin to emerge at 500°C and 650°C, particularly at high pressures, indicating that elevated temperatures and pressures favor the formation of more complex hydrocarbons. These trends reflect the thermodynamic shift driven by pressure toward heavier molecular species and the temperature-driven enhancement of cracking reactions that produce hydrogen and light gases. This aligns with previous work using reactive force field molecular simulations on high-temperature and high-pressure(11.6 MPa and 2000 K) pyrolysis of hexadecane which revealed optimal conditions for ethylene and H_2 formation at specific pressure and temperature ranges, highlighting the complex interplay between these parameters in determining product distributions (Chen et al., 2017).

5. Energy and exergy efficiency analysis of polypropylene pyrolysis

Fig. 4. presents the energy and exergy efficiencies, heat loss, and reaction heat requirement as functions of temperature during polypropylene pyrolysis. The parameters analyzed include the energy and exergy efficiencies of the pyrolysis process and H_2 production, as well as the heat loss and reaction heat requirement. The total exergy efficiency (η_{Ex}^{Total}) remains at ca. 85 %, across the temperature range, indicating consistent energy conversion. The energy efficiency (η_{En}^{Total}) increases steadily from ca. 20 % at lower temperatures to ca. 65 % at 650°C, suggesting that higher temperatures improve overall energy utilization. The exergy efficiency for H_2 production (η_{EX}^{H2}) increases significantly with temperature, reaching a peak of around 35 % at 650°C before slightly declining. This indicates that higher temperatures enhance the quality of energy conversion into H_2. Similarly, the H_2 energy efficiency (η_{En}^{H2}) rises with temperature, peaking at ca. 65 % at 650°C suggesting this is the optimal temperature for energy utilization in H_2 production.

Heat loss (MJh^{-1}kg^{-1}$(\text{-}C_3H_6\text{-})_n$) increases with temperature, rising from near zero at lower temperatures to ca. 1 MJh^{-1}kg^{-1}$(\text{-}C_3H_6\text{-})_n$ at 650°C due to greater thermal losses to the surroundings at higher

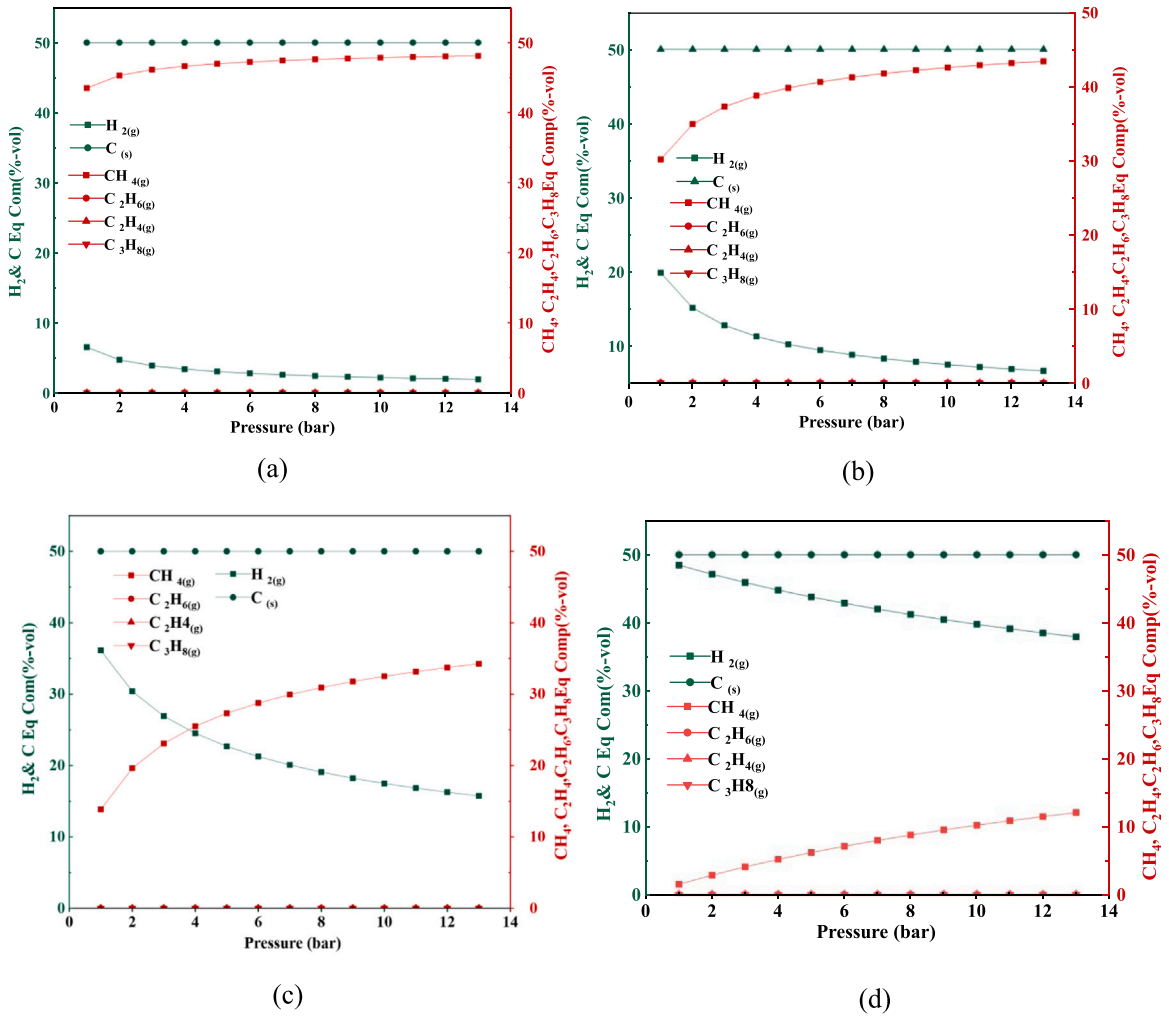

Fig. 3. The equilibrium composition of the pyrolysis reaction as influenced by pressure at a) T = 300℃, b) T = 400℃, c) T = 500℃, d) T = 650℃.

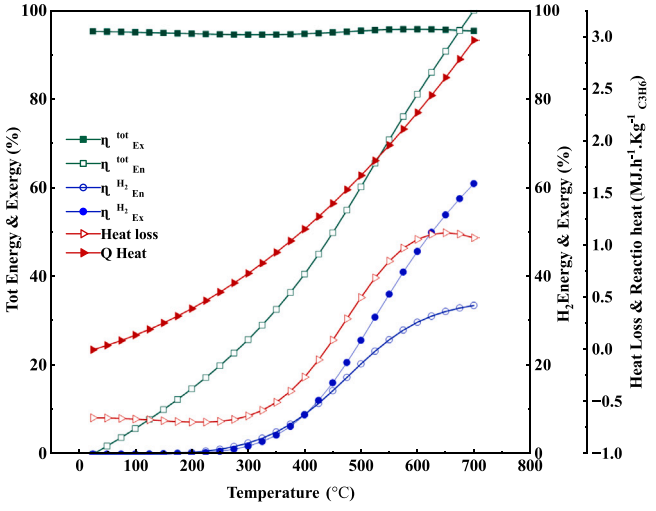

Fig. 4. Energy and exergy efficiencies, heat loss, and reaction heat requirement as functions of temperature during the pyrolysis of polypropylene.

temperatures. The reaction heat requirement also increases with temperature from ca. 1 $MJh^{-1}kg^{-1}_{(-C3H6-)n}$ at lower temperatures to ca. 3 $MJh^{-1}kg^{-1}(-C_3H_6-)_n$ at 650°C, reflecting the endothermic nature of the pyrolysis reaction. These values demonstrate that although heat loss and reaction heat requirements rise with temperature, the efficiency gains (both energy and exergy) outweigh these losses at 650°C, making it the optimal operating temperature for maximizing H_2 production efficiencies. Kim et al. demonstrated that higher pyrolysis temperatures enhance hydrogen yield and energy efficiency despite increased heat loss, confirming that optimized thermal input maximizes overall conversion performance (Kim et al., 2025).

Table 3
Pyrolysis reactor process evaluation.

Reactants	**wt%**	**Flow rate (kg h^{-1})**	**Flow rate (kmol h^{-1})**
$(-C_3H_6-)_n$	**100.00**	**1.00**	**0.02**
Product gases			
	vol%	Flow rate (Nm^3 h^{-1})	Flow rate (kmol h^{-1})
$C_{(s)}$	50.00	1.52	295.69
$H_{2(g)}$	48.48	1.57	0.07
$CH_{4(g)}$	1.52	0.05	0.05
$C_2H_{4(g)}$	0.00	0.00	0.00
$C_2H_{6(g)}$	0.00	0.00	0.00
$C_3H_{8(g)}$	0.00	0.00	0.00
Energy Balance (Gas products)			
	Thermal E flow (MJ h^{-1})	Total H flow (MJ.h^{-1})	Total Exergy flow (MJ h^{-1})
Raw Material	2.61	0.60	47.85
Pyrolysis gas product	1.41	1.25	95.51

Table 3 provides reactant and product gases data, along with the energy balance for polypropylene pyrolysis at optimized conditions (T = 650℃, P = 1 bar) with a reactant flow rate of 1 kg h^{-1} or 0.02 kmol $h^{-1}$of (-C_3H_6-)$_n$. The primary products include 1.57 Nm^3h^{-1} (0.07 kmol.h^{-1}) of H_2 and 0.07 Nm^3 h^{-1} of CH_4 (0.003 kmol.h^{-1}), indicating 48.48 vol% H_2 production with a flow rate corresponding to 0.07 kmol. h^{-1}. The energy balance shows a thermal energy input of 2.61 MJ.h^{-1} and a total exergy flow of 46.73 MJ.h^{-1} (Table 2 ESI) reflecting effective energy utilization and high exergy efficiency in the pyrolysis process. Additionally, the comparison between the thermal energy flow (1.41 MJ h^{-1}) and total enthalpy flow (1.25 MJ h^{-1}) for the pyrolysis gas products, underscores the importance of managing heat losses as it directly influences the energy balance and ensures that a maximum amount of input energy is converted into useful products, rather than being dissipated as waste heat. For H_2 production at this temperature, the energy and exergy efficiencies (57.6 %, and 35 %, respectively) indicate effective conversion of supplied energy into useful chemical energy, further supporting this process's efficiency. Given the high yields of H_2 and the favourable energy and exergy values, producing H_2 through polypropylene pyrolysis does appear to offer a viable pathway for sustainable H_2 production. Although polypropylene pyrolysis involves a complex network of elementary reactions, the current analysis employs global reaction models under thermodynamic equilibrium assumptions. Since exergy is a state function, the computed exergy values primarily depend on the final chemical composition and thermodynamic state, rather than on the reaction pathway (Meramo et al., 2021; Zhang et al., 2020). Therefore, the use of more detailed kinetic mechanisms would be expected to impact product transients or reaction rates but have minimal influence on the equilibrium-based exergy values reported here.

CO_2 and CO Methanation: ΔG-Log K Trends and Product Distribution

Fig. 5a. illustrates the Gibbs free energy change (ΔG) and equilibrium constant (log K) for CO_2 and CO methanation reactions (R_6 and R_7, Table 4) as a function of temperature. Both reactions are thermodynamically favorable below 500 °C, as indicated by negative ΔG values and log K > 1, suggesting high equilibrium conversions. In contrast, reverse water-gas shift (RWGS), and dry reforming of methane (DRM), as detailed in Table 4, remain less favourable up to 650 °C, with less negative or near-zero ΔG. The optimal methanation window lies between 200 °C and 400 °C, where ΔG is minimized and conversion to CH_4 is maximized. At a hydrogen generation rate of ~7 mol h^{-1} from PP pyrolysis, stoichiometric reduction of ~1 mol h^{-1} each of CO and CO_2 is feasible, based on H_2:CO and H_2:CO_2 ratios of 3:1 and 4:1, respectively.

Fig. 5b. shows the equilibrium product distributions across 200–700 °C, supporting the trends observed in Fig. 5a. Maximum CH_4 formation occurs between 250 °C and 400 °C, consistent with the exothermic nature of methanation. Above 400 °C, equilibrium shifts toward CO and H_2, resulting in reduced CH_4 yield. These findings align with established thermodynamic behaviour, where low temperatures Favor methane selectivity in exothermic systems (Rönsch et al., 2016).

As depicted in Fig. 6, at 250°C (a) and 350°C (b), increasing the pressure up to 10 bar further enhances methane production, evidenced by the substantial rise in CH_4 yield and the corresponding decrease in CO and CO_2 concentrations. Additionally, Fig. 6d. shows that at higher temperatures like 550°C, the positive effect of pressure on methane production diminishes, with an increased formation of solid carbon, highlighting the importance of maintaining lower temperatures for optimal results. Moreover, as demonstrated in Fig. 7a, the H_2 flow rate significantly impacts the conversion efficiency of CO and CO_2 into methane up to a point after which excess H_2 does not contribute to higher methane yields but rather results in unreacted H_2. Fig. 7a. further supports this by demonstrating that the conversion rates of CO and CO_2 remain high, while methane yield peaks around 250–400°C and then declines as temperature increases, indicating that there is indeed a stoichiometric balance that must be maintained to optimize the methanation reaction. Recent studies have shown that H_2 flow rates play a critical role in optimizing methane production during methanation processes (Ren et al., 2023; Brooks et al., 2007). Research by Toko et al. (2022) found that while higher H_2 flow rates can increase CO_2 throughput, they may also reduce methane selectivity if not properly balanced. Similarly, Han et al. (2022) demonstrated that adjusting the H_2/CO_2 ratio is essential for maximizing CO_2 conversion and methane productivity, underscoring the importance of carefully controlling hydrogen flow rates in methanation processes.

Fig. 7b. shows the comparison between input and output gases in a methanation process, specifically focusing on how H_2 is utilized to maximize methane production while effectively converting CO and CO_2.

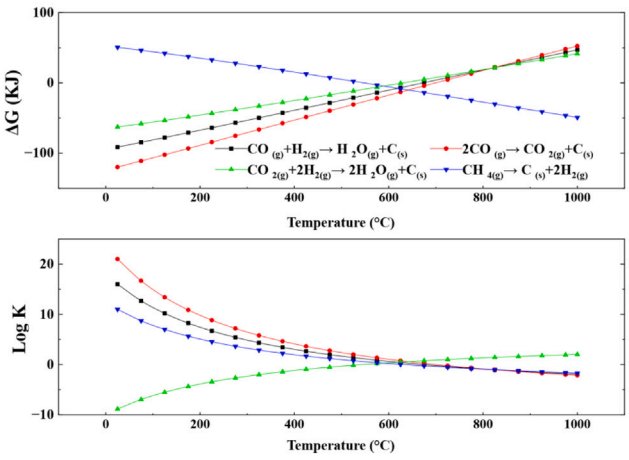

(a)

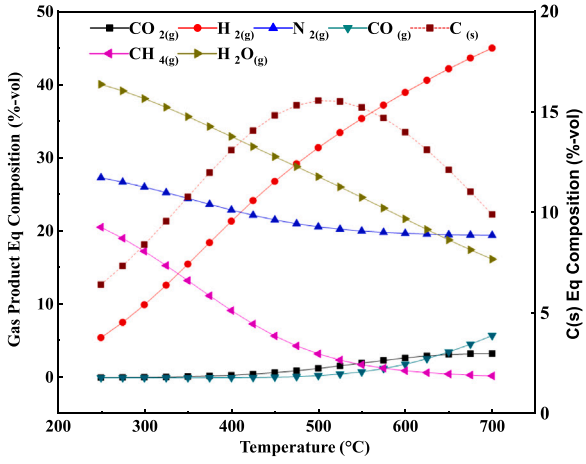

(b)

Fig. 5. (a) the CO_2 and CO methanation and by-product reactions; ΔG-Log K versus temperature, (b) The equilibrium composition of the CO_2 and CO methanation reactions versus temperature at P = 1 bar.

Table 4
Thermodynamic properties and equilibrium constants of various reactions involved in CO_2 methanation reactions.

Reaction	Reaction Equation	ΔH°_{298} (kJ. mol^{-1})	ΔG°_{298} (KJ)	Log K
R_6	$4\,H_{2(g)} + CO_{2(g)} \rightarrow CH_{4(g)} + 2\,H_2O_{(g)}$	−164.74	−113.33	19.85
R_7	$3\,H_{2(g)} + CO_{(g)} \rightarrow CH_{4(g)} + H_2O_{(g)}$	−205.88	−141.93	24.86
R_8	$H_{2(g)} + CO_{2(g)} \rightarrow CO_{(g)} + H_2O_{(g)}$	41.13	28.60	−5.01
R_9	$CH_{4(g)} + CO_{2(g)} \rightarrow 2CO_{(g)} + 2\,H_{2(g)}$	247.02	170.53	−29.87

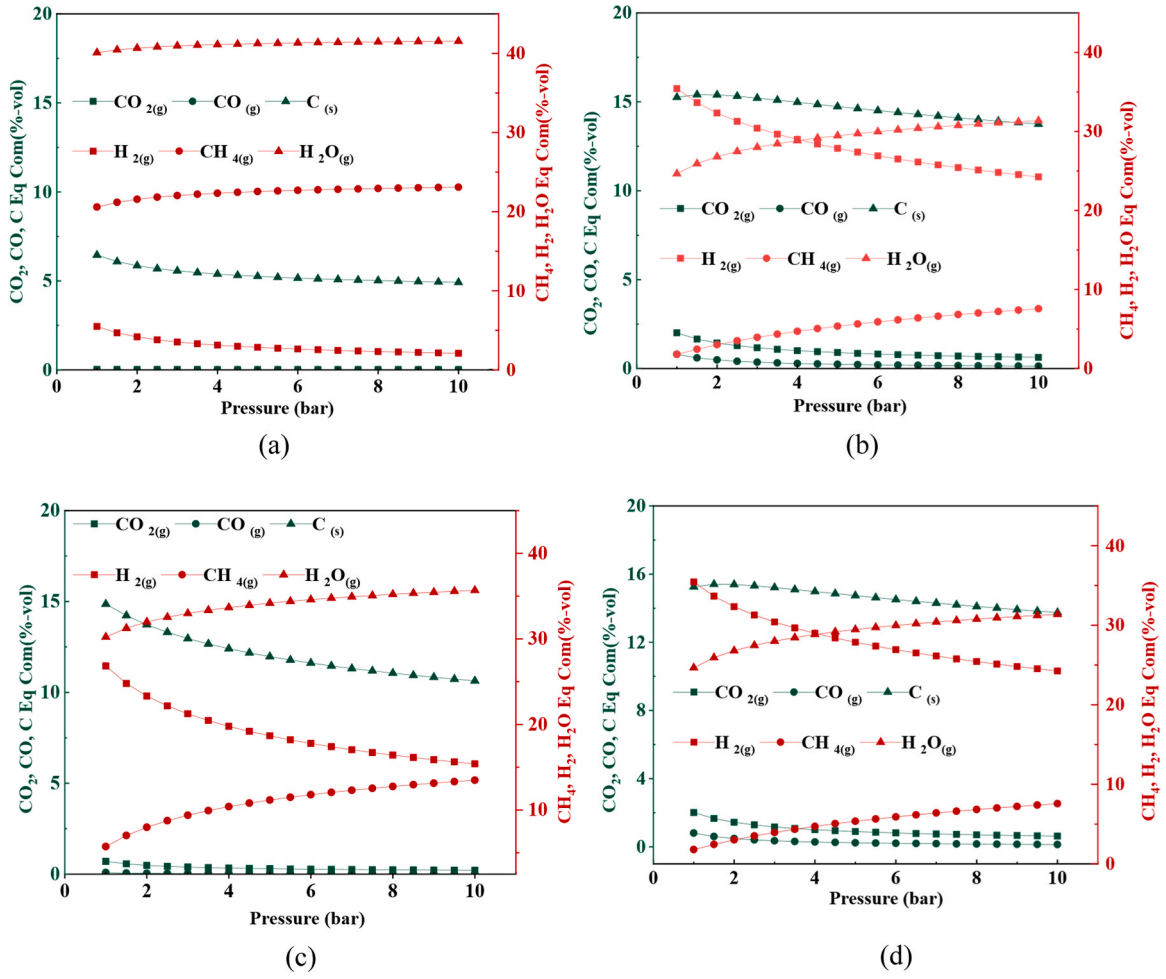

Fig. 6. The equilibrium composition of the CO_2 and CO methanation reaction as influenced by pressure at a) T = 250℃, b) T = 350℃, c) T = 450℃, d) T = 550℃.

The input gas for H_2 aligns with a flow rate of ca. 1. 5 $Nm^3\ h^{-1}$ (7 mol $h^{-1)}$, which is consistent with the flow rate required to optimize methane production when processing a mixed gas containing 1 mol of CO (0.25 $Nm^3\ h^{-1}$) and 1 mol of CO_2 (0.23 $Nm^3\ h^{-1)}$.

The output data shows that this flow rate of H_2 not only supports high CH_4 output but also results in significant amounts of solid carbon and water (H_2O) as by-products. The alignment between the input H_2 and the required flow rate for the methanation process supports the claim that polypropylene pyrolysis, which produces about 7 mol h^{-1} of H_2 can effectively meet the H_2 demand of the process. This ensures that both CO and CO_2 are converted efficiently into methane, aligning well with process requirements and optimizing the overall reaction yield.

Fig. 8. presents the temperature-dependent conversion efficiencies of CO and CO_2, the methane (CH_4) yield, and the carbon balance during the methanation process. At lower temperatures (300–400 °C), CO conversion approaches 100 %, while CO_2 conversion, though slightly lower, remains substantial. As temperature increases beyond 400 °C, conversion efficiencies for both species decline, with a more pronounced drop observed for CO_2. Methane yield follows a similar trend, reaching a maximum of > 95 % between 300–400 °C before decreasing sharply at higher temperatures. This behavior is consistent with the exothermic nature of methanation, which thermodynamically favors product formation at lower temperatures. These observations are in line with reported findings that underscore the strong temperature sensitivity of CO_2 methanation and its competition with CO, particularly under diffusion-limited conditions (Han et al., 2024).

6. Coke formation

Recent studies have shown that carbon formation remains a significant challenge in the CO_2 methanation, affecting both catalyst performance and stability (Han et al., 2024; Mebrahtu et al., 2019). Fig. 9. elaborates on the equilibrium constants and Gibbs free energy of carbon formation and oxidation reactions as a function of temperature. At lower temperatures (T ≤ 400°C), coke formation is more likely, posing a risk for catalyst deactivation. However, at elevated temperatures, carbon formation is significantly suppressed, highlighting temperature's role in mitigating carbon deposition during methanation. The thermodynamic evaluation reveals that the Boudouard reaction ($CO_{(g)} \rightarrow C_{(s)} + CO_{2(g)}$), and the CO/CO_2 reduction reactions ($CO_{(g)} + H_{2(g)} \rightarrow H_2O_{(g)} + C_{(s)}$) have relatively lower equilibrium constants compared to other reactions (Fig. 9a). This implies that these reactions are more prone to changes in operational parameters. As the temperature rises, the Gibbs free energy associated with carbon formation reactions becomes less favourable, while the Gibbs free energy of carbon oxidation reactions becomes increasingly negative. This dynamic shift reduces solid carbon formation at higher temperatures due to enhanced gasification reactions, converting solid carbon into gaseous products such as CO and CO_2.

The carbon balance at T ≤ 300°C remains around 1, which indicates the effective reconversion of solid carbon into gaseous carbonaceous products under methanation reaction conditions. At these lower temperatures, the presence of CO_2 in the input gas further promotes carbon oxidation via the reaction $C_{(s)} + CO_{2(g)} \rightarrow 2CO_{(g)}$, as evidenced by the carbon balance being close to 1 at low temperatures. This oxidation reaction effectively reduces carbon formation, fostering a low-carbon

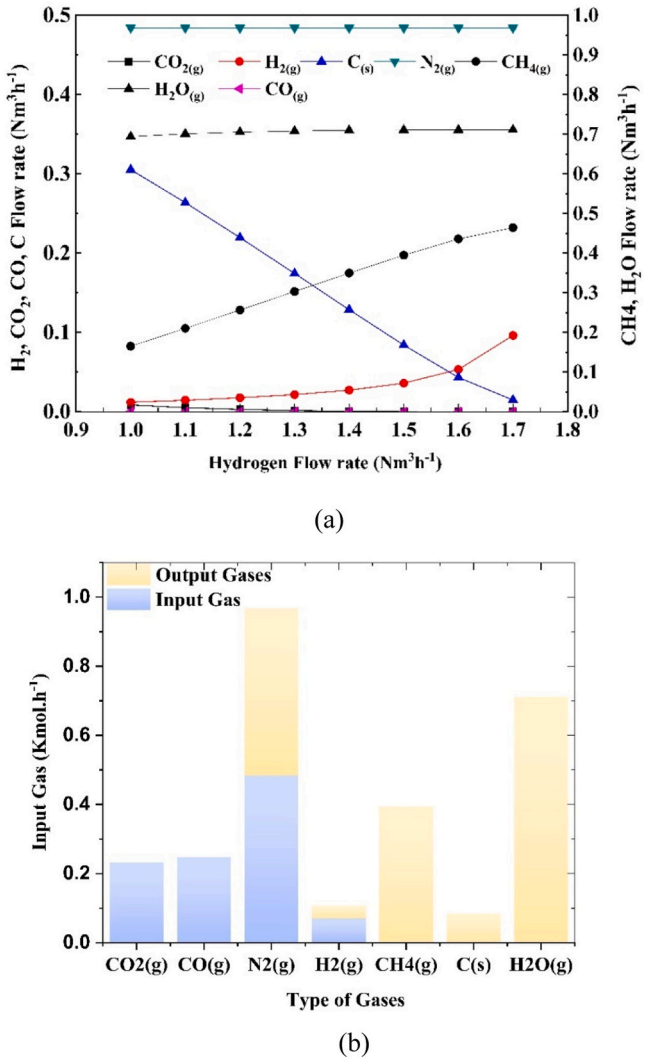

Fig. 7. a) The equilibrium composition of the gases during CO_2 and CO hydrogenation to produce methane as influenced by H_2 flow rate, at T = 250°C and P = 10 bar, b) The equilibrium composition of the input and output gases of the CO and CO_2 methanation reaction.

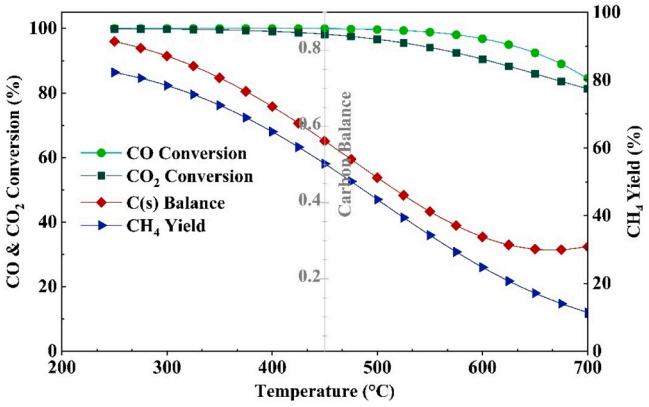

Fig. 8. CO/CO_2 conversion, CH_4 yield and the carbon balance ($CB = \frac{(FCH4_{out} + FCO_{out} + FCO2_{out})}{(FCO2_{in} + FCO_{in})}$) as function of temperature during the methanation reaction.

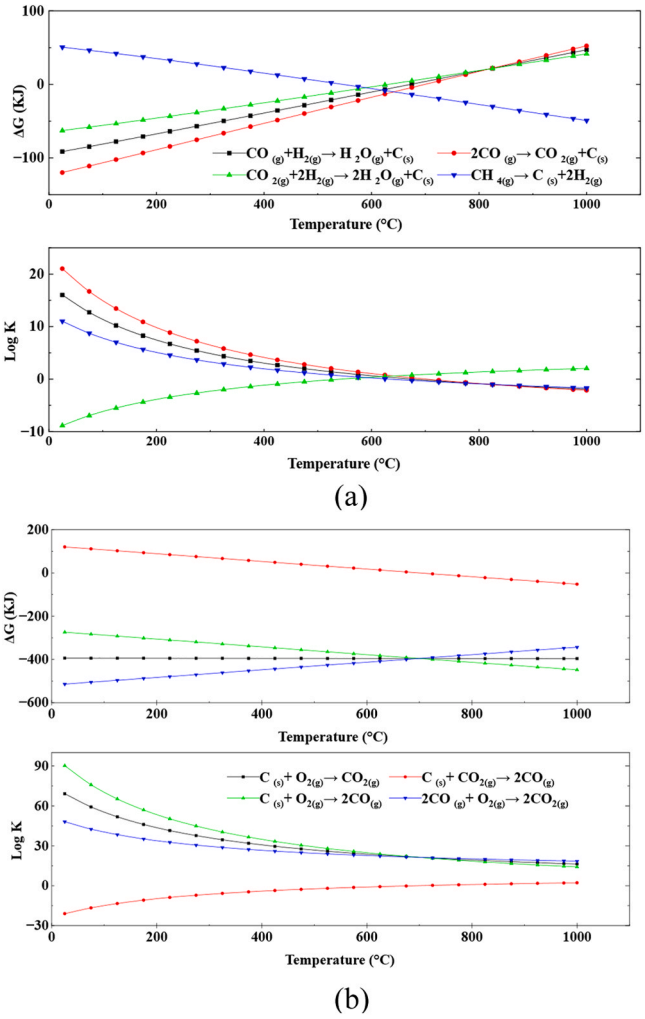

Fig. 9. The equilibrium constants and Gibbs free energy of carbon a) formation, b) oxidation reactions as a function of temperature.

production environment. Consequently, achieving zero-carbon formation is more feasible in this lower temperature regime, and at higher temperatures, carbon deposition is further suppressed, allowing for stable catalyst performance over extended operation. This thermodynamic trend is consistent with the findings of Gao et al. (2012), that demonstrated that carbon deposition primarily from the Boudouard reaction and CO/CO_2 reduction pathways—is favored at low temperatures but becomes significantly suppressed at elevated temperatures due to the increasing dominance of carbon oxidation and gasification reactions, which convert solid carbon into CO and CO_2 as Gibbs free energy becomes more negative.

3. *Energy and Exergy Efficiency Analysis of CO_2 and CO methanation*

Analysis of the effects of H_2 flow rate and temperature on energy and exergy efficiency for the methane synthesis (Fig. 10a) shows that increasing H_2 flow rate from 1.0 to 1.8 $Nm^3\ h^{-1}$ improves total energy efficiency from ca. 48–59 % and synthesis energy efficiency from ca. 14–30 %. Total exergy efficiency rises from ca. 53–91 %, and synthesis exergy efficiency from ca. 43–80 %. Heat loss decreases as the H_2 flow rate increases, indicating more efficient energy use at higher H_2 flow rates, while the heat requirement remains stable across different flow rates.

Fig. 10b. details the effect of temperature on these efficiencies showing total energy efficiency peaks at ca. 100 % at 400°C, where the

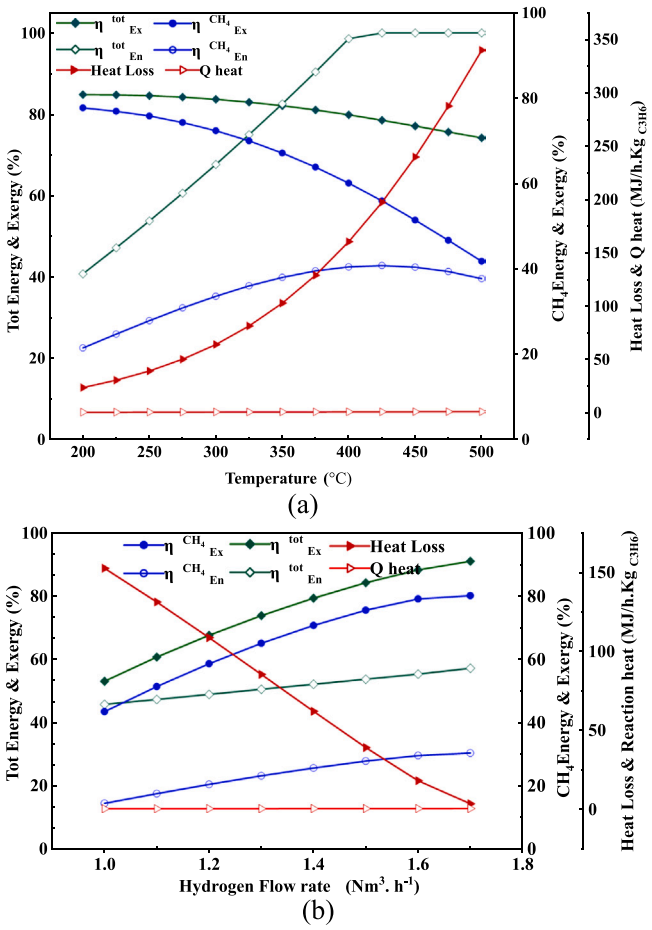

Fig. 10. Energy and exergy efficiencies, heat loss, and reaction heat requirement as functions of a) H_2 flow rate, b) Temperature during the CO and CO_2 methanation reaction.

synthesis energy efficiency reaches ca. 40 %. Total exergy efficiency remains relatively constant at approximately 85 %, but synthesis exergy efficiency declines from about 78–40 % as temperature increases from 200°C to 500°C indicating low methane flow rate as temperature increases. Heat loss increases with temperature, highlighting higher thermal losses at elevated temperatures, yet the heat requirement stays relatively constant.

The energy and exergy efficiencies observed in this study are consistent with recent findings in the field of methane synthesis and CO_2 methanation processes. Mendoza-Hernandez et al. (2019) report the exergy efficiency of a water electrolyze thermally coupled with a CO_2 hydrogenation reactor reaches its peak (70 %) at 200°C and 0.1 MPa for an H_2/CO_2 molar ratio of 4, demonstrating the significant impact of thermal coupling on overall system efficiency. Similarly, for an H_2/CO_2 molar ratio of 2, the peak exergy efficiency was slightly lower, around 68 %, and occurred at a Sabatier temperature of approximately 340°C at 0.1 MPa. These values highlight the critical importance of optimizing temperature and pressure conditions to maximize exergy efficiency in methane synthesis processes.

7. Conclusions

This study introduces a thermochemical pathway that merges hydrogen production from polypropylene (PP) waste with methanation of steelmaking off-gases, offering a dual solution to two pressing industrial challenges: plastic pollution and metallurgical CO/CO_2 emissions. Through detailed Gibbs free energy minimization, we demonstrate that hydrogen derived from PP pyrolysis yielding up to 7 mol h^{-1} flow rate with high energy and exergy efficiencies (65.6 % and 35 %, respectively), providing a clean and storable reductant for carbon conversion. This hydrogen stream, when fed into a catalyst-free methanation process operating between 250–400 °C and 10 bar, enables complete conversion of CO and CO_2 into methane with selectivity exceeding 80 %, and minimal coke formation. The coupling of these processes not only enhances thermodynamic and exergy performance but also closes resource loops by transforming two carbon-intensive waste streams into a valuable synthetic fuel.

The concept reframes waste as a distributed energy vector: plastic polymers become hydrogen reservoirs; steelmaking off-gases become carbon carriers for synthetic fuel. In doing so, the process aligns with net-zero objectives and decarbonization targets across both energy and materials sectors. While further investigation into kinetics, scale-up integration, and economic viability is required, the thermodynamic evidence establishes a compelling foundation for reimagining industrial waste streams as interconnected nodes in a closed-loop, carbon-resilient energy future.

CRediT authorship contribution statement

Peter J. Holliman: Writing – review & editing, Writing – original draft, Validation, Supervision, Software, Resources, Project administration, Funding acquisition, Data curation. **Azita Etminan:** Writing – review & editing, Writing – original draft, Visualization, Validation, Software, Resources, Project administration, Methodology, Investigation, Formal analysis, Data curation, Conceptualization. **Ciaran Martin:** Writing – review & editing, Validation, Supervision, Software, Resources, Funding acquisition. **Ian Mabbett:** Writing – review & editing, Software, Resources, Investigation, Funding acquisition, Data curation. **Chay Davies-Smith:** Writing – review & editing, Validation, Resources, Data curation, Conceptualization.

Funding sources

We gratefully thank EPSRC and Tata Steel for co-sponsoring an iCASE PhD studentship (Voucher number 220106) for AE and EPSRC for funding the Sustain Hub (EP/S018107/1) for PJH.

Declaration of Competing Interest

We have no conflicts of interests to disclose.

Acknowledgment

The authors would like to express their gratitude to Ehsan Akbari Kharaji for his exceptional creativity and dedication in designing the graphical abstract for this paper. His thoughtful work and creativity helped clearly illustrate the key concepts of our research.

Appendix A. Supporting information

Supplementary data associated with this article can be found in the online version at doi:10.1016/j.egyr.2025.05.043.

Data Availability

Data will be made available on request.

References

Ahmadian, E., Schmidt, R.-R., 2020. Exergy analysis of district energy systems and comparison of their exergetic, energetic and environmental performance. Int. J. Exergy 32, 103–129.

Al-Asadi, M., Miskolczi, N., Eller, Z., 2020. Pyrolysis-gasification of wastes plastics for syngas production using metal modified zeolite catalysts under different ratio of nitrogen/oxygen. J. Clean. Prod. 271, 122186.

Al-Juboori, O., Sher, F., Khalid, U., Niazi, M.B.K., Chen, G.Z., 2020. Electrochemical production of sustainable hydrocarbon fuels from CO2 co-electrolysis in eutectic molten melts. ACS Sustain. Chem. Eng. 8, 12877–12890.
Alper, E., Orhan, O.Y., 2017. CO2 utilization: developments in conversion processes. Petroleum 3, 109–126.
Angeli, S.D., Gossler, S., Lichtenberg, S., Kass, G., Agrawal, A.K., Valerius, M., Kinzel, K. P., Deutschmann, O., 2021. Reduction of CO(2) emission from off-gases of steel industry by dry reforming of methane. Angew. Chem. Int. Ed. Engl. 60, 11852–11857.
Aresta, M., Dibenedetto, A., 2024. Merging the green-H2 production with carbon recycling for stepping towards the carbon cyclic economy. J. CO2 Util. 80, 102688.
Bailera, M., Lisbona, P., Peña, B., Romeo, L.M., 2021. A review on CO2 mitigation in the iron and steel industry through power to X processes. J. CO2 Util. 46.
Bampaou, M., Panopoulos, K., Seferlis, P., Sasiain, A., Haag, S., Wolf-Zoellner, P., Lehner, M., Rog, L., Rompalski, P., Kolb, S., Kieberger, N., Dettori, S., Matino, I., Colla, V., 2022. Economic evaluation of renewable hydrogen integration into steelworks for the production of methanol and methane. Energies 15.
Brooks, K.P., Hu, J., Zhu, H., Kee, R.J., 2007. Methanation of carbon dioxide by hydrogen reduction using the Sabatier process in microchannel reactors. Chem. Eng. Sci. 62, 1161–1170.
Büker, K., Von Morstein, O., Yildirim, Ö., Frey, A., Voss, C., Geisbauer, A., 2022. Practical aspects of converting steel mill gases to chemical feedstocks. Chem. Ing. Tech. 94, 1452–1457.
Chen, J., Guo, Y., Wu, X., 2024. Challenges of hydrogen production from biomass gasification. Sustainable Development of Renewable Energy. Elsevier.
Chen, Z., Sun, W., Zhao, L., 2017. High-temperature and high-pressure pyrolysis of hexadecane: molecular dynamic simulation based on reactive force field (ReaxFF). J. Phys. Chem. A 121, 2069–2078.
Dermühl, S., Riedel, U., 2023. A comparison of the most promising low-carbon hydrogen production technologies. Fuel 340, 127478.
Gao, J., Wang, Y., Ping, Y., Hu, D., Xu, G., Gu, F., Su, F., 2012. A thermodynamic analysis of methanation reactions of carbon oxides for the production of synthetic natural gas. RSC Adv. 2, 2358–2368.
García-Nieto, P.J., García-Gonzalo, E., Paredes-Sánchez, B.M., Paredes-Sánchez, J.P., 2023. Modelling hydrogen production from biomass pyrolysis for energy systems using machine learning techniques. Environ. Sci. Pollut. Res. 30, 76977–76991.
Han, D., Cho, W., Baek, Y., 2022. CO2 Methanation of biogas over Ni-Mg-Al: the effects of Ni content, reduction temperature, and biogas composition. Catalysts 12, 1054.
Han, X., Ostrikov, K.K., Chen, J., Zheng, Y., Xu, X., 2023. Electrochemical reduction of carbon dioxide to solid carbon: development, challenges, and perspectives. Energy Fuels 37, 12665–12684.
Han, W., Shujia, G., Zhangfeng, Q., Zhikai, L., Guofu, W., Mei, D., Weibin, F., Jianguo, W., 2024. A thermodynamic consideration on the synthesis of methane from CO, CO2, and their mixture by hydrogenation. J. Fuel Chem. Technol. 52, 1453–1461.
Hos, T., Herskowitz, M., 2021. Utilization of CO-rich waste gases from the steel industry for production of renewable liquid fuels. Energy Convers. Manag. 240.
Hussain, I., Jalil, A., Hassan, N., Hamid, M., 2021. Recent advances in catalytic systems for CO2 conversion to substitute natural gas (SNG): perspective and challenges. J. Energy Chem. 62, 377–407.
Jia, Y., Zhou, Z., Chen, D., Li, E., Jiang, Z., Zhao, L., Guo, L., 2024. Recent advances in molten salt CO2 capture and electrochemical conversion to functional carbon materials. J. Ind. Eng. Chem. 134, 17–27.
Jiang, Q., Xin, Y., Xing, J., Sun, X., Long, Y., Hong, H., Xu, C., 2024. Performance of iron-based perovskite-type oxides for chemical looping dry reforming of methane. Energy Fuels 38, 21189–21203.
Jin, B., Wei, K., Ouyang, T., Fan, Y., Zhao, H., Zhang, H., Liang, Z., 2023. Chemical looping CO2 capture and in-situ conversion: fundamentals, process configurations, bifunctional materials, and reaction mechanisms. Appl. Energy Combust. Sci. 16, 100218.
Kakoee, A., Gharehghani, A., 2020. Carbon oxides methanation in equilibrium; a thermodynamic approach. Int. J. Hydrog. Energy 45, 29993–30008.
Khor, S., Jusoh, M., Zakaria, Z., 2022. Hydrogen production from steam and dry reforming of methane-ethane-glycerol: a thermodynamic comparative analysis. Chem. Eng. Res. Des. 180, 178–189.
Kim, D., Lee, S., Woo, S.-Y., Park, K.Y., 2025. Enhanced hydrogen production through temperature-optimized pyrolysis of mixed plastic waste for sustainable energy recovery. Process Saf. Environ. Prot. 196, 106934.
Kim, Y.-M., Pyo, S., Hakimian, H., Yoo, K.-S., Rhee, G.-H., Park, Y.-K., 2021. Kinetic analysis for the catalytic pyrolysis of polypropylene over low cost mineral catalysts. Sustainability 13, 13386.
Kim, J., Sovacool, B.K., Bazilian, M., Griffiths, S., Lee, J., Yang, M., Lee, J., 2022. Decarbonizing the iron and steel industry: a systematic review of sociotechnical systems, technological innovations, and policy options. Energy Res. Soc. Sci. 89.
Liu, X., Burra, K.G., Wang, Z., Li, J., Che, D., Gupta, A.K., 2020b. On deconvolution for understanding synergistic effects in co-pyrolysis of pinewood and polypropylene. Appl. Energy 279, 115811.
Liu, J., Jiang, Z., Yu, H., Tang, T., 2011. Catalytic pyrolysis of polypropylene to synthesize carbon nanotubes and hydrogen through a two-stage process. Polym. Degrad. Stab. 96, 1711–1719.
Liu, H., Wang, C., Zhang, J., Zhao, W., Fan, M., 2020a. Pyrolysis kinetics and thermodynamics of typical plastic waste. Energy Fuels 34, 2385–2390.
Martínez-Rodríguez, A., Abánades, A., 2020. Comparative analysis of energy and exergy performance of hydrogen production methods. Entropy 22, 1286.
Mebrahtu, C., Krebs, F., Abate, S., Perathoner, S., Centi, G., Palkovits, R., 2019. CO2 methanation: principles and challenges. Studies in Surface Science and Catalysis. Elsevier.
Melo Bravo, P., Jiménez, R., Devred, F., Debecker, D.P., Ulloa, C., García, X., 2020. Kinetics of CO methanation using a Fe-bearing catalyst from a blast furnace sludge. Fuel 276.
Mendoza-Hernandez, O.S., Shima, A., Matsumoto, H., Inoue, M., Abe, T., Matsuzaki, Y., Sone, Y., 2019. Exergy valorization of a water electrolyzer and CO2 hydrogenation tandem system for hydrogen and methane production. Sci. Rep. 9, 6470.
Mensah, I., Ahiekpor, J., Bensah, E., Narra, S., Amponsem, B., Antwi, E., 2022. Recent development of biomass and plastic co-pyrolysis for syngas production. Chem. Sci. Int. J. 31, 41–59.
Meramo, S., Puello, P., Rodríguez, J., 2021. Sustainability outlook of thermochemical-based second-generation biofuel production: exergy assessment. Appl. Sci. 11, 8851.
Najera, M., Solunke, R., Gardner, T., Veser, G., 2011. Carbon capture and utilization via chemical looping dry reforming. Chem. Eng. Res. Des. 89, 1533–1543.
Patlolla, S.R., Katsu, K., Sharafian, A., Wei, K., Herrera, O.E., Mérida, W., 2023. A review of methane pyrolysis technologies for hydrogen production. Renew. Sustain. Energy Rev. 181, 113323.
Ren, J., Lou, H., Xu, N., Zeng, F., Pei, G., Wang, Z., 2023. Methanation of CO/CO2 for power to methane process: fundamentals, status, and perspectives. J. Energy Chem. 80, 182–206.
Rönsch, S., Schneider, J., Matthischke, S., Schlüter, M., Götz, M., Lefebvre, J., Prabhakaran, P., Bajohr, S., 2016. Review on methanation–from fundamentals to current projects. Fuel 166, 276–296.
Rubinsin, N.J., Karim, N.A., Timmiati, S.N., Lim, K.L., Isahak, W.N.R.W., Pudukudy, M., 2024. An overview of the enhanced biomass gasification for hydrogen production. Int. J. Hydrog. Energy 49, 1139–1164.
Saeidi, S., Najari, S., Hessel, V., Wilson, K., Keil, F.J., Concepción, P., Suib, S.L., Rodrigues, A.E., 2021. Recent advances in CO2 hydrogenation to value-added products—current challenges and future directions. Prog. Energy Combust. Sci. 85, 100905.
Sani, Y.M., Solangi, N.H., Bello, T.K., Isa, M.T., 2023. Perovskite-based nanomaterials for CO2 conversion. Nanomaterials for Carbon Dioxide Capture and Conversion Technologies. Elsevier.
Su, Y., Chen, C.O.-K., 2006. Exergetic efficiency optimization of a refrigeration system with multi-irreversibilities. Proc. Inst. Mech. Eng. Part C J. Mech. Eng. Sci. 220, 1179–1187.
Toko, S., Ideguchi, M., Hasegawa, T., Okumura, T., Kamataki, K., Takenaka, K., Koga, K., Shiratani, M., Setsuhara, Y., 2022. Effect of gas flow rate and discharge volume on CO2 methanation with plasma catalysis. Jpn. J. Appl. Phys. 61, SI1002.
Usman, M., Garba, M.D., Zeb, Z., Israr, M., Safia, S., Javed, F., Suliman, M.S., Alfaify, B., Sanhoob, M.A., Iqbal, N., 2023. Co2 conversion via catalytic hydrogenation to methanol. DME and syngas. Sustainable Utilization of Carbon Dioxide: From Waste to Product. Springer.
Varvoutis, G., Lampropoulos, A., Mandela, E., Konsolakis, M., Marnellos, G.E., 2022. Recent advances on CO2 mitigation technologies: on the role of hydrogenation route via green H2. Energies 15, 4790.
Weiland, F., Qureshi, M.S., Wennebro, J., Lindfors, C., Ohra-Aho, T., Shafaghat, H., Johansson, A.-C., 2021. Entrained flow gasification of polypropylene pyrolysis oil. Molecules 26, 7317.
Wolf-Zoellner, P., Medved, A.R., Lehner, M., Kieberger, N., Rechberger, K., 2021. In Situ catalytic methanation of real steelworks gases. Energies 14, 8131.
Wu, C., Williams, P.T., 2009. Investigation of Ni-Al, Ni-Mg-Al and Ni-Cu-Al catalyst for hydrogen production from pyrolysis–gasification of polypropylene. Appl. Catal. B Environ. 90, 147–156.
Younas, M., Shafique, S., Hafeez, A., Javed, F., Rehman, F., 2022. An overview of hydrogen production: current status, potential, and challenges. Fuel 316, 123317.
Zhang, Y., Ji, G., Ma, D., Chen, C., Wang, Y., Wang, W., Li, A., 2020. Exergy and energy analysis of pyrolysis of plastic wastes in rotary kiln with heat carrier. Process Saf. Environ. Prot. 142, 203–211.
Zhang, L., Jia, C., Bai, F., Wang, W., An, S., Zhao, K., Li, Z., Li, J., Sun, H., 2024. A comprehensive review of the promising clean energy carrier: Hydrogen production, transportation, storage, and utilization (HPTSU) technologies. Fuel 355, 129455.
Zhao, S., Luo, Y., Li, C., Ren, K., Zhu, Y., Dou, W., 2023. High-performance photothermal catalytic CO2 reduction to CH4 and CO by ABO3 (A= La, Ce; B= Ni, Co, Fe) perovskite nanomaterials. Ceram. Int. 49, 20907–20919.
Zhou, Z., Sun, Z., Duan, L., 2023. Chemical looping: a flexible platform technology for CH4 conversion coupled with CO2 utilization. Curr. Opin. Green. Sustain. Chem. 39, 100721.
Zhu, Q., Zeng, Y., Zheng, Y., 2023. Overview of CO 2 capture and electrolysis technology in molten salts: operational parameters and their effects. Ind. Chem. Mater. 1, 595–617.